Applied Surface Science 480 (2019) 131–137

Contents lists available at ScienceDirect

Applied Surface Science

journal homepage: www.elsevier.com/locate/apsusc

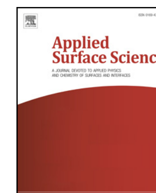

Full length article

Facile fabrication of periodic arrays of vertical Si nanoholes on (001)Si substrate with broadband light absorption properties

Y.M. Tseng[a], R.Y. Gu[a], C.W. Chang[a], S.L. Cheng[a,b,*]

[a] Department of Chemical and Materials Engineering, National Central University, Chung-Li District, Taoyuan City, Taiwan, Republic of China
[b] Institute of Materials Science and Engineering, National Central University, Chung-Li District, Taoyuan City, Taiwan, Republic of China

ARTICLE INFO

Keywords:
Nanosphere lithography
Au nanodisk
Au-catalyzed etching
Si nanohole
Broadband absorption

ABSTRACT

This study presents a facile and straightforward approach to fabricating periodic arrays of Au nanodisks and vertically aligned, depth- and morphology-controllable Si nanoholes on (001)Si substrates by combining self-assembled nanosphere lithography, selective Au wet etching, and Au nanodisk-catalyzed Si etching processes. All of the etching experiments were carried out in aqueous solutions at room temperature without using complex photolithography and hard-mask patterning processes. The shape, diameter, and spacing of the produced vertical Si nanoholes corresponded well to those of the catalytic Au nanodisks used, and the nanohole depth could be readily tuned from sub-micrometer to several micrometers by adjusting the Au nanodisk-catalyzed Si etching time. The Si substrates with nanohole-textured surfaces exhibited depth-dependent hydrophobic behaviors and broadband (400–1650 nm) light absorption properties. The measured integrated absorptance was found to increase with increasing the depth of Au nanodisk-embedded Si nanoholes and can reach up to 95% in the visible light region and 60% in the near-IR region. The resulting broadband absorption enhancement can be attributed to the combined effects of multiple scattering of light and localized surface plasmon resonance. The obtained results present the exciting prospects that the new combined approach proposed here would offer potential applications in constructing various high-efficiency nanohole array-based optoelectronic and photovoltaic devices.

1. Introduction

Recently, single-crystalline Si substrate with nanohole-textured surface has attracted a lot of attention because it possesses excellent light-trapping property and compatibility with the conventional semiconductor process as well as potential applications in advanced photodetectors and photovoltaic devices [1–3]. However, due to the intrinsic bandgap limitation of Si (1.12 eV), the Si crystal is transparent to infrared (IR) light and thus thought not suitable for optical communications. Thus, many recent research efforts have been devoted to fabricating surface-textured Si nanostructures which attempt to extend their light absorption range from the visible to the near-IR region. To produce large-area nanohole and/or nanopore structures on the surfaces of Si substrates, various physical (e.g. ion bombardment etching, silicide sublimation) [4,5], chemical (e.g. alkaline etching, metal-assisted chemical etching) [6–8], and electrochemical (e.g. anodic etching) [9,10] fabrication techniques have been developed. However, the precise controls of size, depth, shape, and location of the Si nanoholes produced by the above-mentioned methods are still the major challenges.

It is known that for practical optoelectronic device applications, dense arrays of ordered surface nanostructures with controlled morphology and dimension need to be fabricated. Therefore, to overcome the above technical challenges, a self-assembly nanopatterning technique known as colloidal nanosphere lithography combined with metal hard mask and wet chemical etching processes was proposed [11–13]. Although this nanosphere-templated wet etching approach has been applied to produce well-ordered Si nanohole arrays on Si substrates, this approach is still limited by the necessity of using additional metal hard mask deposition and stripping processes. Recently, we have developed an alternative nanosphere patterning approach, which combined the oxygen-plasma modified nanosphere lithography and KOH anisotropic etching to produce periodic Si nanohole arrays on differently oriented Si substrates. No additional metal hard mask process is needed in this approach [14,15]. However, the produced Si nanoholes were found to be shallow and heavily faceted. Since the surface

* Corresponding author at: Department of Chemical and Materials Engineering, National Central University, Chung-Li District, Taoyuan City, Taiwan, Republic of China.
E-mail address: slcheng@ncu.edu.tw (S.L. Cheng).

https://doi.org/10.1016/j.apsusc.2019.02.204
Received 20 December 2018; Received in revised form 21 February 2019; Accepted 22 February 2019
Available online 23 February 2019
0169-4332/ © 2019 Elsevier B.V. All rights reserved.

wettability and optical absorption properties of Si nanostructures were known to be strongly affected by their height (depth) and morphology, it is of great importance to develop a low-cost, high-throughput nanopatterning approach to fabricate vertically-aligned Si nanohole arrays with well-controlled depth, morphology, and periodicity and to investigate their corresponding microstructure-dependent properties.

In this study, we propose a novel, facile, and efficient approach, which is based on the oxygen-plasma modified nanosphere lithography in conjunction with the Au nanodisk-catalyzed Si etching process, to fabricate depth-, spacing-, and morphology-controllable, vertically-aligned Si nanohole arrays on (001)Si substrates at room temperature. The whole fabrication processes of Au nanodisk and Si nanohole arrays are carried out in aqueous solution without the need of using additional metal hard masks and complicated apparatuses. The results from a systematic investigation of the morphological evolution, surface wettability, and optical characteristics (400–1650 nm) of Au nanodisks and vertical Si nanohole arrays produced under different wet chemical etching conditions are reported.

2. Experimental procedures

Fig. 1 shows the schematic illustration of the whole fabrication procedure. Square pieces $10 \times 10\ mm^2$ in size were cut from 1 to 10 Ω-cm, boron-doped (001)-oriented silicon wafers and used as the starting substrates. All of these (001)Si substrates were cleaned chemically using a standard procedure and then dipped in a dilute HF solution to remove the surface native oxide layer, prior to being loaded into an electron-beam evaporation system. The base pressure in the deposition chamber was better than 2×10^{-6} Torr. A 30-nm-thick catalytic Au thin film was deposited onto the HF-dipped (001)Si substrates at the deposition rate of 0.04 nm/s. Subsequently, a self-assembled, closely-packed monolayer of polystyrene (PS) nanospheres with a mean diameter of 1000 nm was prepared and transferred to the surface of the Au thin film-coated (001)Si (Au/(001)Si) substrates according to the floating-transferring technique described elsewhere [16,17]. Oxygen plasma etching was then employed to slightly trim the diameter of the PS nanospheres to desirable levels.

After the O_2 plasma treatment, the hexagonal nonclosely-packed PS nanosphere monolayer-masked Au/(001)Si samples were immersed into a $SC(NH_2)_2/Fe(NO_3)_2/H_2O$ mixture solution for various time periods to etch the Au thin film. During the wet chemical etching process, the O_2 plasma trimmed-PS nanospheres acted as etching masks, preventing the underlying Au thin film from being etched. Once the honeycomb-shaped area of the Au thin film which was not masked by the nonclosely-packed PS nanosphere monolayer has been etched, the obtained samples were dipped in tetrahydrofuran (THF) solvent to remove the PS nanospheres, and the periodic Au nanodisk arrays were thus produced on (001)Si substrate. Subsequently, the Au nanodisk-catalyzed Si etching was carried out in a mixed aqueous HF and H_2O_2 solution to produce vertical Si nanohole arrays. In this study, all of the above experimental procedures are performed at room temperature.

A scanning electron microscope (SEM, Hitachi S-3000H, operated at 10 keV) and an atomic force microscope (AFM, SII Technology SPA-400, operated in tapping mode) were utilized to examine the size, depth, periodicity, and surface morphology and roughness of the Au nanodisks and vertical Si nanoholes produced at various etching conditions. An energy dispersion spectrometer (EDS, Bruker XFlash 5010) attached to the SEM was utilized for the determination of chemical composition. The surface wetting properties of the various Si nanohole samples were characterized by water contact angle measurements. A deionized water droplet of about 4 μL was used for each contact angle measurement. The optical properties of the Si substrates with periodic arrays of Au nanodisks and vertical Si nanoholes were determined in the wavelength range of 400–1650 nm using an ultraviolet-visible (UV–Vis) spectrophotometer (PerkinElmer Lambda-35) and a near-infrared (NIR) spectrophotometer (Rainbow-Light TRL-03), both equipped with an integrating sphere accessory.

3. Results and discussion

Fig. 2(a) and (b) show, respectively, the planview SEM images of a self-assembled PS nanosphere monolayer on the surface of the Au/(001)Si substrate before and after appropriate O_2 plasma treatments. It is clearly seen from the insets of Fig. 2(a) and (b) that the diameter of PS nanospheres was reduced uniformly from 1000 nm to 800 nm, and the produced nonclosely-packed PS nanosphere array still remained its original hexagonal periodicity. The obtained hexagonally-ordered O_2 plasma trimmed-PS nanosphere monolayer was then utilized as the etching mask for the subsequent Au etching process. Fig. 2(c)–(f) show the planview SEM images of PS nanosphere-masked Au/(001)Si samples etched in the Au etchant with stirring for different periods of time. As can be seen in these SEM images, the nonclosely-packed PS

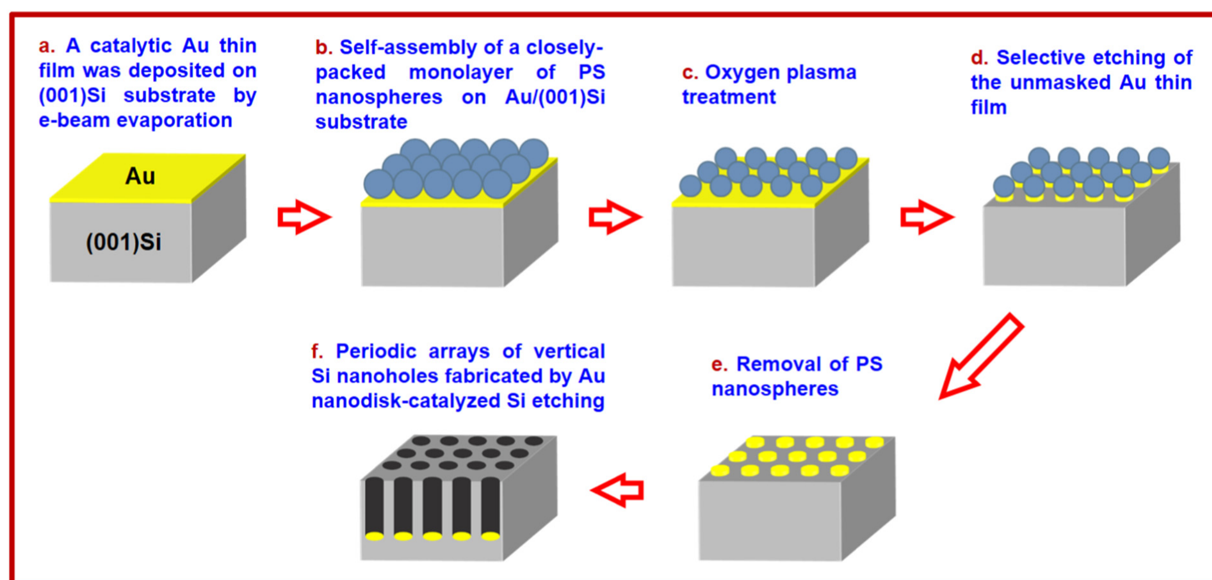

Fig. 1. Schematic illustration of the experimental procedures for the fabrication of periodic arrays of vertically-aligned Au nanodisk-embedded Si nanoholes on (001) Si substrates.

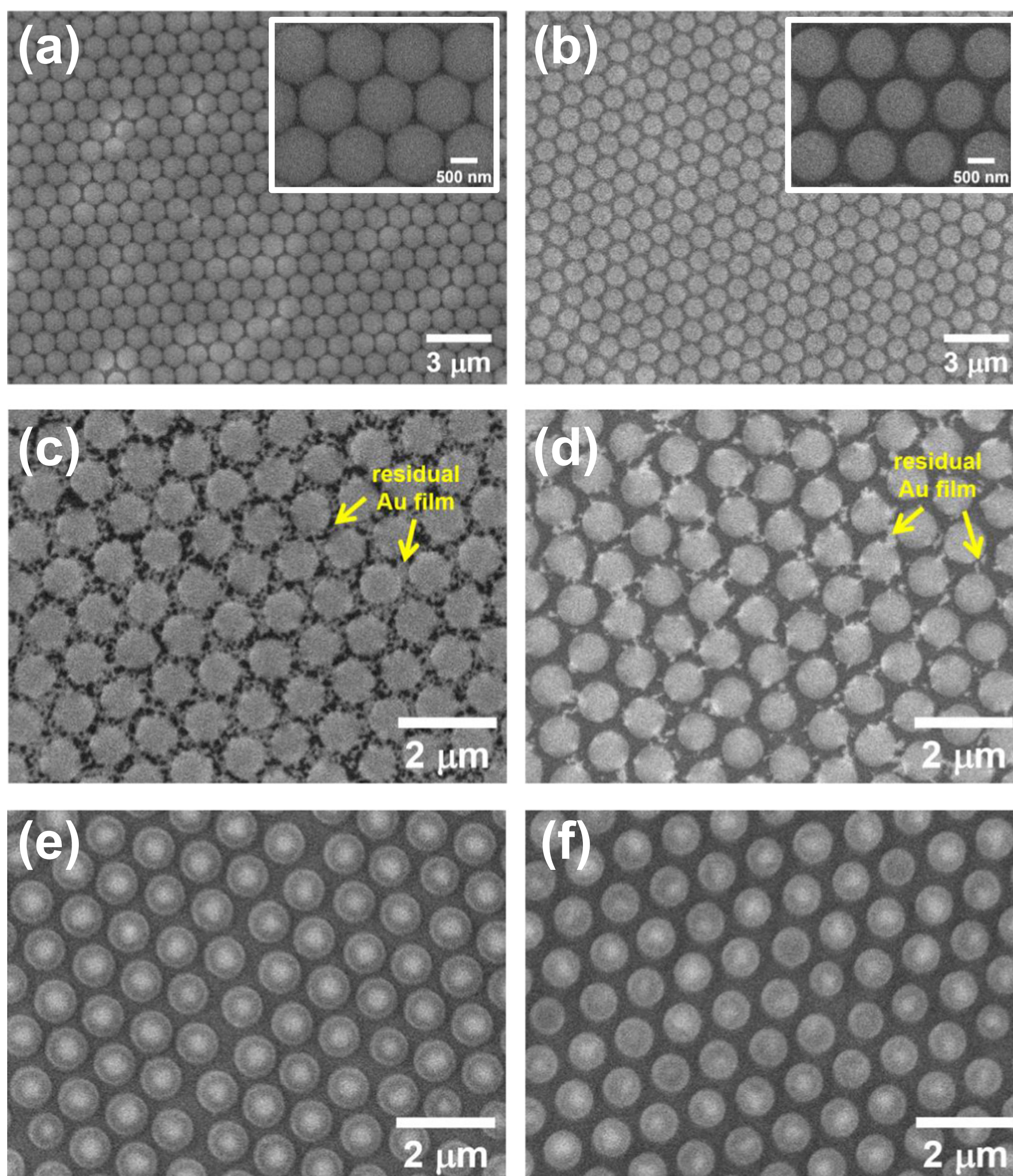

Fig. 2. Planview SEM images of a 1000-nm-diameter PS nanosphere monolayer on Au/(001)Si substrate (a) before and (b) after the O_2 plasma treatment. The insets are the corresponding high-magnification SEM images. Planview SEM images of nonclosely-packed PS nanosphere array-masked Au/(001)Si samples etched in the Au etchant for (c) 3 min, (d) 5 min, (e) 7 min, and (f) 8 min.

nanosphere masks effectively protect the underlying Au thin film from being etched, only allowing the exposed Au area to be etched, resulting in the formation of circular disk-shaped Au layer under each PS nanosphere (the area with brighter contrast). The detailed reaction mechanism for the etching of Au thin films in a $SC(NH_2)_2/Fe(NO_3)_2/H_2O$ mixture solution can be found in previous studies [18,19]. In order to examine clearly the morphological evolution of the Au nanodisk array with the etching time, the PS nanosphere masks were removed by dissolving in THF solvent after each Au etching run. From SEM examinations, as shown in Fig. 3(a) and (b), we can see that the Au etching reaction starts in the honeycomb-shaped region of the Au thin film that was not masked by the O_2 plasma trimmed-PS nanospheres, and then propagates laterally. For the PS nanosphere-masked Au/(001) Si samples after etching for 7 min, a periodic array of circular Au nanodisks with a mean diameter of 500 nm was successfully produced on (001)Si substrates. An example is shown in Fig. 3(c). It should be mentioned here that as the etching time was further increased to 8 min (Fig. 3(d)), some of the Au nanodisks were found to be etched away. The observed results were also confirmed by EDS analyses. Fig. 3(e) shows the EDS spectra acquired from the regions (i) and (ii) marked by yellow crosses in Fig. 3(c). As shown in Fig. 3(e), there were no Au signals detected in the region (ii) that was not masked by the O_2 plasma trimmed-PS nanospheres, indicating that for the sample after etching in the Au etchant for 7 min, the exposed Au film was etched completely. Moreover, from the above SEM results, the diameter of the produced Au nanodisks was found to decrease with increasing the etching time; however, their center-to-center spacing and periodicity remained almost the same as that of the PS nanosphere masks used in this study. Fig. 3(f) shows a representative AFM image and the corresponding line-scan profile of a periodic array of 500-nm-diameter Au nanodisks, showing that the surface of Au nanodisks was relatively smooth with a surface roughness (R_a) being about 1.5 nm. In addition, the thickness of the produced Au nanodisks is uniform and measured to be approximately 30.2 nm, which is close to that of the blanket Au thin film

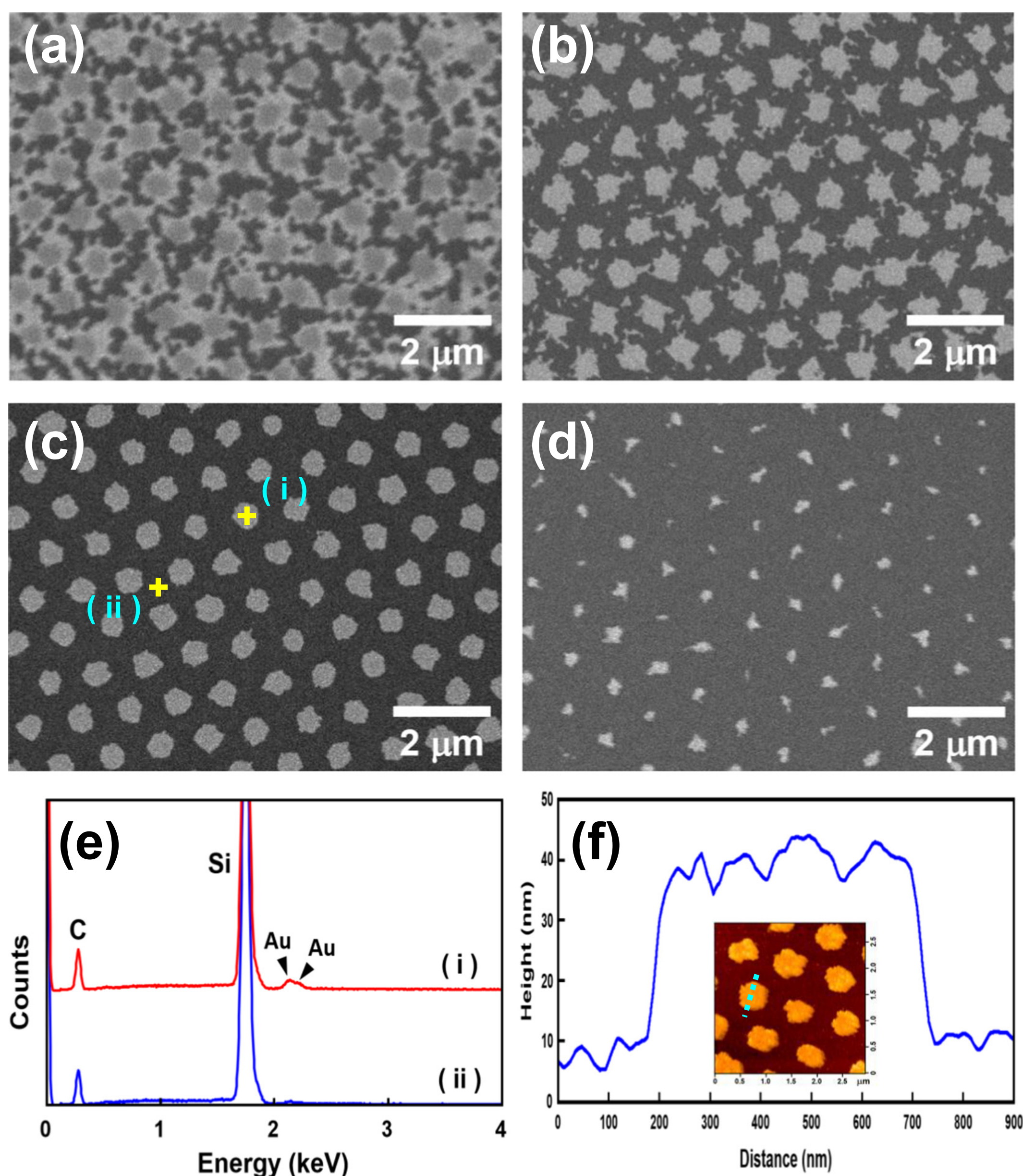

Fig. 3. Planview SEM images of periodic Au nanodisk arrays produced on (001)Si substrate with etching times of (a) 3 min, (b) 5 min, (c) 7 min, and (d) 8 min. (e) The corresponding spot EDS spectra acquired from the regions (i) and (ii) marked by yellow crosses in (c). (f) The corresponding AFM image and line-scan profile of (c).

deposited. The produced 500-nm-diameter circular Au nanodisks were then used as the catalysts to fabricate a periodic array of Si nanoholes on (001)Si substrate via the Au-catalyzed Si etching process [20–22].

Fig. 4(a)–(c) are the representative planview SEM images showing the morphological evolution of the Si nanohole arrays with the Au-catalyzed Si etching time at room temperature. The corresponding tilted-view SEM images are shown in Fig. 4(d)–(f). As can be seen from the SEM observations, the catalytic Au nanodisks were lying at the nanohole bottoms and all of the produced Au nanodisk-embedded Si nanoholes were circular in shape and vertically aligned in relation to the (001)Si substrate surface. In addition, the nanohole diameter was rather uniform over the entire depth and measured to be about 500 nm, corresponding well to that of the produced Au nanodisks. The observed results clearly demonstrate that, in contrast to other etching approaches, no additional hard masks deposition and stripping processes are needed for our proposed new approach, and the diameter of the vertical Si nanoholes can be well controlled by the size of the produced Au nanodisks. The SEM images also reveal that the depth of the Si nanoholes increases with the duration of the etching process. Fig. 4(g) shows the plot of the depth of vertical Si nanoholes produced as a function of the Au-catalyzed Si etching time. The relation curve is nearly linear, indicating that in the range of etching conditions studied here, the Au-catalyzed Si etching process is entirely reaction controlled, and the depth of Si nanoholes can be readily tuned by adjusting the Au-catalyzed Si etching time.

Fig. 5 shows the variation of water contact angles for the HF-dipped (001)Si substrates before and after the formation of vertical Si nanohole arrays. The insets are the corresponding photo images of deionized water droplets on the sample surfaces with different depths of Si nanoholes. It is found that the measured water contact angle values significantly increase from initial ~85° (blank Si) to 113°–135° (nanohole depth: 0.35–0.6 μm), and reach to ~140° with increasing the nanohole depth up to 1.5 μm or more, indicating that the surfaces of the Si substrates with vertical Si nanohole arrays have a greater hydrophobicity

Applied Surface Science 480 (2019) 131–137

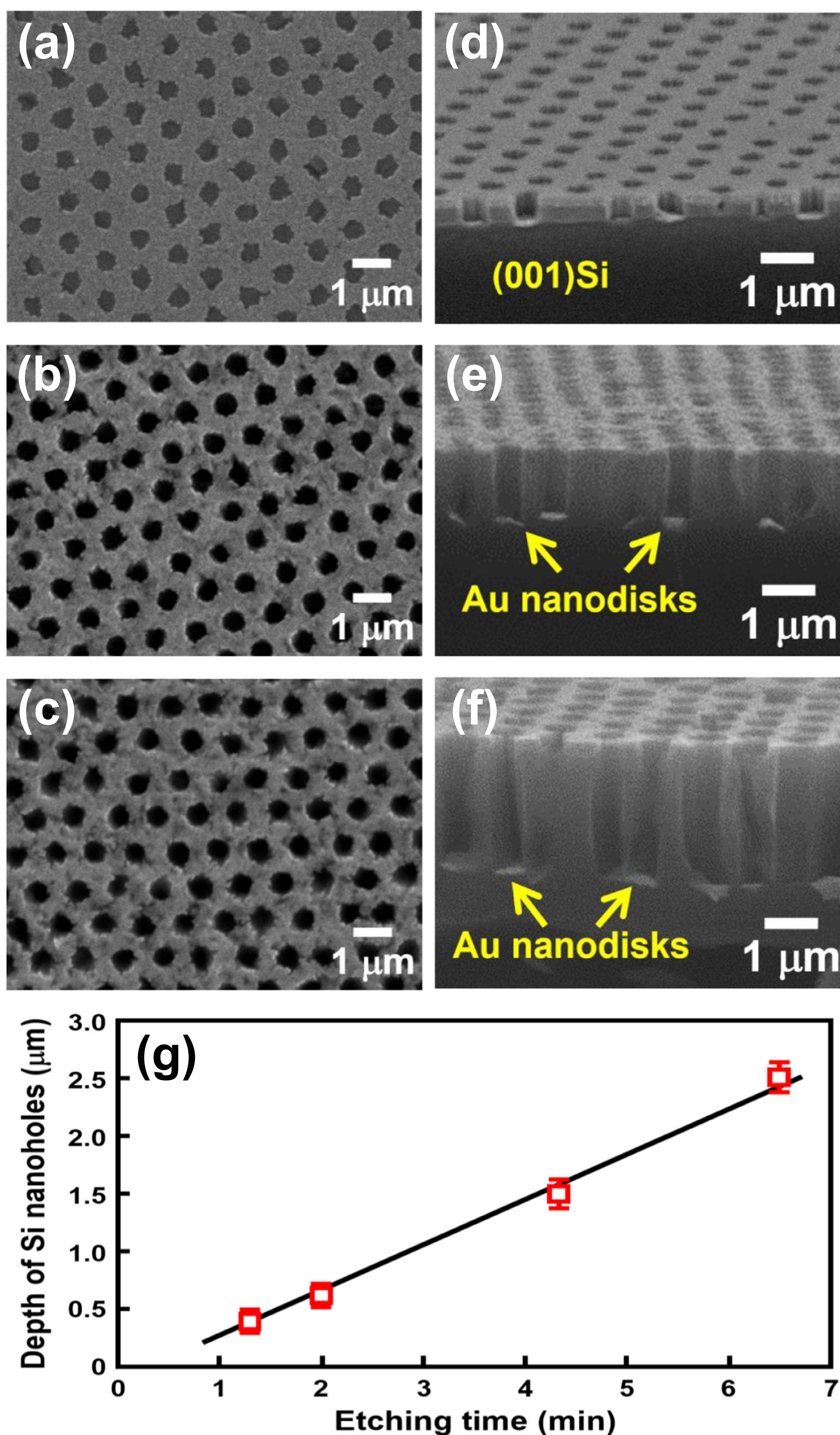

Fig. 4. Planview and the corresponding tilted-view SEM images of periodic arrays of vertical Si nanoholes fabricated by Au nanodisk-catalyzed Si etching for (a) (d) 2 min, (b) (e) 4.3 min, and (c) (f) 6.5 min. (g) A plot of the average depth of vertical Si nanoholes versus the Au nanodisk-catalyzed Si etching time.

compared to that of the HF-dipped bare Si substrate. The enhanced hydrophobicity was associated with the vertical nanohole structure and H-terminated Si surface and could be explained by the Cassie-Baxter model [23]. According to this model, when a water droplet is deposited on the hydrophobic H-terminated Si nanohole surface, air would be trapped in nanoholes underneath the water droplet. The presence of a large amount of trapped air would prevent water from intruding into the nanoholes, leading to an increased surface hydrophobicity of the nanohole-structured Si substrates.

In order to investigate the light absorption characteristics of the produced periodic arrays of vertical Si nanoholes with varying depths, the integrated reflectance (R %) and transmittance (T %) were measured using a UV–Vis-NIR spectrometer equipped with an integrated sphere. Fig. 6(a) and (b) show, respectively, the corresponding

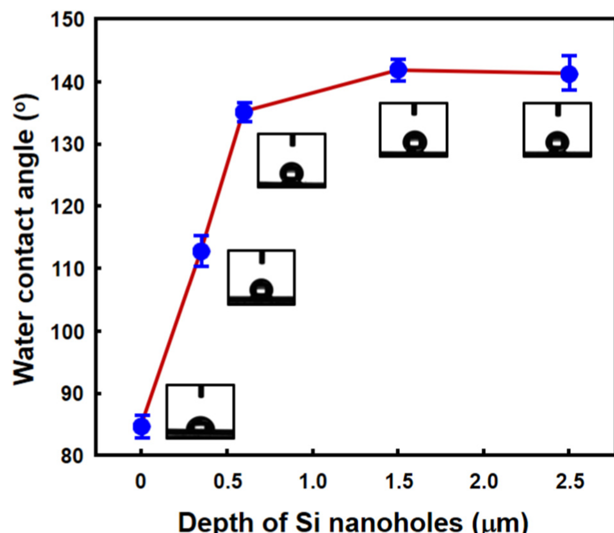

Fig. 5. The variation of water contact angle with the depth of the produced vertical Si nanohole arrays. The insets are the corresponding photographs of water droplets on the sample surfaces.

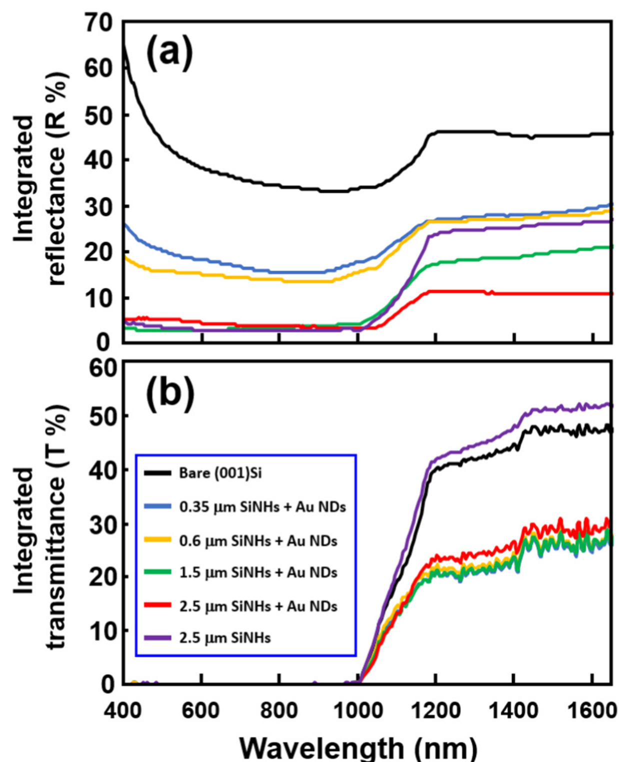

Fig. 6. (a) Integrated reflection and (b) transmission spectra of bare (001)Si substrates with different types of vertical nanohole structures (SiNHs: Si nanoholes, AuNDs: Au nanodisks).

integrated reflection and transmission spectra in the wavelength ranges of 400–1650 nm. From the measured reflection spectra shown in Fig. 6(a), we can see that compared with the flat bare Si substrate (R % ~ 33–65%), the surface reflectances of all the Si samples with Si nanohole arrays were significantly reduced over the entire spectral range. In addition, the measured integrated reflectance was found to gradually decrease with increasing the depth of Au nanodisk-embedded Si nanoholes. It is worth noting that as the embedded Au nanodisks were removed by dissolving in an aqua regia solution, the corresponding integrated reflectance was increased, especially in the near-IR region (although it was still lower than that of the bare Si substrate). On the other hand, since silicon has a bandgap of 1.12. eV at room temperature it is substantially transparent to wavelengths greater than 1100 nm. Thus, it can be expected that the decrease of the integrated reflectance in the near-IR region would lead to an increase in light transmission. As can be seen in Fig. 6(b), the near-IR transmittance of the vertical Si nanohole array without the embedded Au nanodisks is indeed higher than that of the bare Si substrate due to its reduced reflectance. However, in analyzing the Au nanodisk-embedded Si nanohole arrays, the measured transmission spectra (Fig. 6(b)) instead revealed that the decrease of the integrated reflectance in the near-IR region (Fig. 6(a)) does not lead to an increase but a decrease in the near-IR transmission. The abnormal decreased near-IR transmission phenomenon was obviously associated with the presence of the embedded Au nanodisk arrays. By measuring the integrated reflectance (R %) and transmittance (T %) from Fig. 6, the integrated light absorptance (A %) can be readily determined by the equation: A % = 100% - R % - T %. The corresponding integrated absorption spectra of different types of nanohole-textured Si samples are shown in Fig. 7. It is apparent from Fig. 7 that the integrated absorptance of blank-(001)Si substrate in the range of 400 to 1650 nm was significantly enhanced by the formation of vertically-aligned, periodic Au nanodisk-embedded Si nanohole arrays. Compared with the blank-Si substrate and other nanohole-textured Si samples, the Si sample with a 2.5-μm-depth Si nanohole structure and embedded Au nanodisks exhibited the highest broadband absorption, where the integrated absorptance exceeded 95% in the visible light region and 60% in the near-IR region. The resulting broadband absorption enhancement can be attributed to the combined effects of the deep vertical nanohole structures, which result in strong light trapping through multiple scattering, and the embedded metallic Au nanodisks, which result in light confinement through localized surface plasmon resonance [24–26].

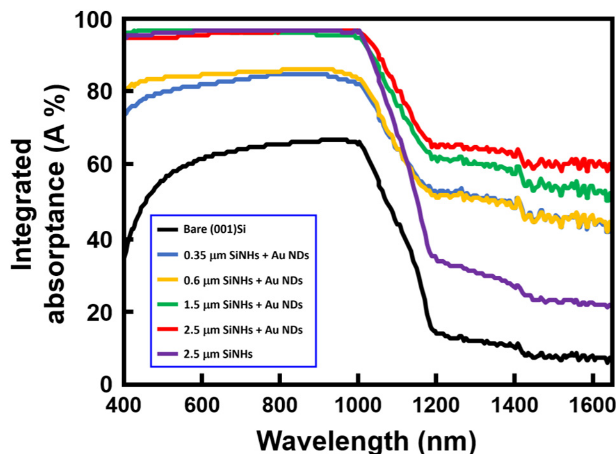

Fig. 7. The integrated absorption spectra of bare (001)Si substrates with different types of vertical nanohole structures (SiNHs: Si nanoholes, AuNDs: Au nanodisks).

4. Summary and conclusions

In summary, periodic arrays of vertically aligned, diameter-, depth-, and morphology-controllable Si nanoholes have been successfully produced on (001)Si substrates by using the Au nanodisk-catalyzed Si etching approach proposed in this study. The catalytic Au nanodisks with controlled diameter were prepared via self-assembled nanosphere lithography and selective Au wet etching process without the need of using additional metal hard masks. The formation kinetic of Si nanohole was found to follow the reaction-controlled process, and the nanohole depth could be readily tuned by adjusting the Au nanodisk-catalyzed Si etching time. Compared with the blank-Si substrate, the

produced Au nanodisk-embedded Si nanohole structures exhibit not only improved hydrophobicity from 85° to 140°, but also greatly enhanced light absorption in the wavelength range of 400 to 1650 nm. Since the diameter, interspacing, and depth of the produced Si nanoholes can be readily controlled by adjusting the Au nanodisk-catalyzed Si etching conditions and the diameters of PS nanospheres and Au nanodisks, the room-temperature fabrication approach proposed here provides a facile and novel strategy to fabricate a variety of nanohole array-based broadband optoelectronic devices.

Acknowledgment

The research was supported by the Ministry of Science and Technology of Taiwan, R.O.C.

References

[1] C. Xie, X.J. Zhang, K.Q. Ruan, Z.B. Shao, S.S. Dhaliwal, L. Wang, Q. Zhang, X.W. Zhang, J.S. Jie, J. Mater. Chem. A 1 (2013) 15348.
[2] Y. Gao, H. Cansizoglu, K.G. Polat, S. Ghandiparsi, A. Kaya, H.H. Mamtaz, A.S. Mayet, Y.A. Wang, X.Z. Zhang, T. Yamada, E.P. Devine, A.F. Elrefaie, S.Y. Wang, M.S. Islam, Nat. Photonics 11 (2017) 301.
[3] S.H. Altinoluk, H.E. Ciftpinar, O. Demircioglu, F. Es, G. Baytemir, O. Akar, A. Aydemir, A. Sarac, T. Akin, R. Turan, Energy Procedia 92 (2016) 291.
[4] H.S. Lee, J.K. Suk, H.Y. Kim, J.K. Kim, J.H. Song, D.S. Jeong, J.K. Park, W.M. Kim, D.K. Lee, K.J. Choi, B.K. Ju, T.S. Lee, I.H. Kim, Sci. Rep. 8 (2018) 3504.
[5] H.T. Wang, Z. Zhang, L.M. Wong, S.J. Wang, Z.P. Wei, G.P. Li, G.Z. Xing, D.L. Guo, D.D. Wang, T. Wu, ACS Nano 4 (2010) 2901.
[6] A. Mavrokefalos, S.E. Han, S. Yerci, M.S. Branham, G. Chen, Nano Lett. 12 (2012) 2792.
[7] S.H. Altinoluk, H.E. Ciftpinar, O. Demircioglu, R. Turan, J. Mater Sci, Nanotechnol 5 (2017) 2348.
[8] S.C. Shiu, S.C. Hung, H.J. Syu, C.F. Lin, J. Electrochem. Soc. 158 (2011) D95.
[9] Y.M. Wu, X.Z. Zhang, J.S. Jie, C. Xie, X.W. Zhang, B.Q. Sun, Y. Wang, P. Gao, J. Phys. Chem. C 117 (2013) 11968.
[10] X.J. Shen, L. Chen, J.N. Li, J. Zhao, J. Power Sources 318 (2016) 146.
[11] C.H. Sun, W.L. Min, N.C. Linn, P. Jiang, Appl. Phys. Lett. 91 (2007) 231105.
[12] J.Y. Ji, H.Q. Zhang, Y. Qiu, L. Wang, Y. Wang, L.H. Hua, Appl. Surf. Sci. 292 (2014) 86.
[13] C.G. Wang, X.Z. Wu, D. Di, P.T. Dong, R. Xiao, S.Q. Wang, Nanoscale 8 (2016) 4672.
[14] S.L. Cheng, Y.H. Lin, S.W. Lee, T. Lee, H. Chen, J.C. Hu, L.T. Chen, Appl. Surf. Sci. 263 (2012) 430.
[15] S.L. Cheng, Y.H. Lin, S.W. Lee, H. Chen, Thin Solid Films 557 (2014) 376.
[16] C.L. Zhang, S. Cvetanovic, J.M. Pearce, MethodsX 4 (2017) 229.
[17] P.I. Stavroulakis, N. Christou, D. Bagnall, Mater. Sci. Eng. B 165 (2009) 186.
[18] J.S. Li, J.D. Miller, Hydrometallurgy 89 (2007) 279.
[19] T. Groenewald, J. South. Afr. Inst. Min. Metall. 11 (1977) 217.
[20] L.Y. Li, Y. Liu, X.Y. Zhao, Z.Y. Lin, C.P. Wong, Appl. Mater. Interfaces 6 (2014) 575.
[21] H.D. Um, N.W. Kim, K.M. Lee, I.C. Hwang, J.H. Seo, Y.J. Yu, P. Duane, M. Wober, K.Y. Seo, Sci. Rep. 5 (2015) 11277.
[22] B. Miao, J. Zhang, X. Z. Ding, D. M. Wu, Y. H. Wu, W. H. Lu, and J. D. Li, J. Micromech. Microeng. 27 (2017) 055019.
[23] A.B.D. Cassie, S. Baxter, Trans. Faraday Soc. 4 (1944) 546.
[24] B.S. Kim, S.H. Tamboli, J.B. Han, T.H. Kim, H.H. Cho, Int. J. Heat Mass Transf. 82 (2015) 267.
[25] K. Liu, S.C. Qu, X.H. Zhang, F.R. Tan, Z.U. Wang, Nanoscale Res. Lett. 8 (2013) 88.
[26] K.T. Lin, H.L. Chen, Y.S. Lai, C.C. Yu, Nat. Commun. 5 (2014) 3288.